Investigating the effect of a wave-dependent momentum flux in a process oriented ocean model

Björn Carlsson, Anna Rutgersson and Ann-Sofi Smedman

Department of Earth Sciences (Air, Water and Landscape Sciences), Uppsala University, Villavägen 16, SE-752 36 Uppsala, Sweden

Carlsson, B., Rutgersson, A. & Smedman, A.-S. 2009: Investigating the effect of a wave-dependent momentum flux in a process oriented ocean model. *Boreal Env. Res.* 14: 3–17.

New expressions of the drag coefficient were developed using measurements from the Östergarnsholm site in the Baltic Sea. The drag coefficient was significantly lower in the presence of waves travelling faster than the wind (swell). The expressions were implemented in an oceanographic process-oriented model in a 45-year simulation. Since no wave information was included we did an analysis of the potential impact of swell on an ocean model. Current velocity and surface stress were significantly altered during periods with low wind speed but the temperature and the mixing depth in the ocean were not significantly changed. The implementation of the swell effect in a process oriented ocean model is thus of limited importance. There is, however, an indication that for studies of current velocity it is crucial to have a correct description of the drag coefficient.

Introduction

When modelling the atmosphere as well as the ocean it is of crucial importance to correctly describe the boundary conditions. The atmosphere–ocean boundary is an important source of turbulence in the atmosphere as well as in the ocean and there is a significant exchange of momentum, heat and moisture. The turbulence in the ocean is mainly generated by surface waves and current shear governed by the surface stress, and controls the depth of the ocean mixed layer together with the heat fluxes.

Traditionally the atmospheric surface layer is described by the Monin-Obukhov Similarity Theory (MOST). It assumes stationary and homogeneous conditions and a solid surface. Numerous field measurements have confirmed MOST over land (e.g. Businger *et al*. 1971,

Haugen *et al*. 1971, Högström 1990) as well as over the ocean (Smedman *et al*. 1994, Guo Larsén *et al*. 2003). However, several investigations in the marine surface layer have found important deviations in the applicability of MOST (Smedman *et al*. 1994, Smedman *et al*. 1999, Rutgersson *et al*. 2001). The surface is not solid but changing as a response to the atmospheric forcing. In the wave boundary layer (WBL) the waves directly influence the atmospheric turbulence. Above the viscous sub-layer the total wind stress or momentum flux τ can be expressed as:

$$\tau = \tau_t + \tau_w = \rho_a u_*^2 \qquad (1)$$

Here τ_t is the turbulent part, τ_w the wave induced part and $u_* = [(\overline{-u'w'})^2 + (\overline{-v'w'})^2]^{1/4}$ is the measured friction velocity, with u', v' and w' being

the longitudinal, lateral and vertical wind fluctuations, respectively (bar denoting the Reynolds average); and ρ_a is the air density.

The wind stress is generally described by a bulk formulation, where the friction velocity is related to the wind speed by a bulk coefficient according to:

$$\frac{\tau}{\rho_a} = u_*^2 = C_D U_{10}^2 \qquad (2)$$

where C_D is the drag coefficient and U_{10} the mean wind speed at 10 m. The drag coefficient depends on the sea surface roughness and the atmospheric stability. The neutral drag coefficient C_{DN}, valid for neutral stratification, is a function only of the roughness parameter z_0. Smoother surface yields a smaller C_{DN}. Several parameterisation studies arrive at a wind speed dependent C_{DN} (e.g. Large and Pond 1981, Jansen *et al.* 1987, Fairall *et al.* 2003). An alternative way to calculate z_0 and thus C_{DN} is to use the Charnock equation $z_0 = \alpha u_*^2/g$ (Charnock 1955), where α is the Charnock parameter and g is the gravitational acceleration. Some studies show the Charnock parameter depending on the state of the waves (e.g. Drennan *et al.* 2003).

The state of the waves can be described by wave age c_p/U_{10}, where c_p is the phase speed of the dominant waves. The definition of wave age sometimes includes a factor $1/\cos\beta$, where β is the angle between the local wind and the waves. This would give unrealistic results since, for swell waves, this factor can be very large. It would imply increasing atmospheric effects with increasing values of $1/\cos\beta$, predictions which disagree with our data for the approximate range $\beta < 90°$. As a result we choose not to include the $\cos\beta$ term here.

According to Pierson and Moskowitz (1964) and Pierson (1964) the wave age at which the waves are fully developed is $c_p/U_{10} = 1.2$. We differentiate between three wave states:

Growing sea: $c_p/U_{10} < 0.8$
Mixed sea: $0.8 < c_p/U_{10} < 1.2$
Swell: $c_p/U_{10} = 1.2$

For growing sea conditions, when the wind is feeding the waves with energy, the WBL is of the order of 1 m.

During swell the waves are not generated by the local wind. This is often the case during a decaying storm or when waves are transported from a distant storm. Since the swell can travel long distances without dissipating it has been assumed that there is no transport of energy from the waves to the wind. However, during swell the WBL is significantly deeper and the structure in the whole boundary layer could be affected (Smedman *et al.* 1994, Smedman *et al.* 1999). Effects of swell on the turbulence structure in the overlying airflow are supported by both DNS (direct numerical simulation) (Sullivan *et al.* 2000, Rutgersson and Sullivan 2005) and LES (large eddy simulation) (Sullivan *et al.* 2008).

One of the effects of swell is seen in the drag coefficient. In most investigations analysing measurements during swell the scatter of C_{DN} increases significantly. When the swell direction follows the wind direction (following swell) the drag coefficient is reduced (Guo Larsén *et al.* 2003 and Drennan *et al.* 1999a). When the swell is cross or against the wind direction (cross/counter swell) C_{DN} has been seen to increase (Guo Larsén *et al.* 2003, Drennan *et al.* 1999a). This can be explained by τ_w, which gives an upward contribution of momentum during following swell, that is, wave energy is transported from the waves to the wind. The physical mechanism is, however, not yet fully understood. The turbulent contribution, τ_t, always gives a negative momentum transport and for further increase of the wave age there can be a sign reversal of $\tau_t + \tau_w$, i.e. a net positive upward momentum transport (Smedman *et al.* 1999, Grachev and Fairall 2001). Other deviations from MOST observed in the presence of swell include a low level wind maximum (Holland *et al.* 1981, Donelan 1990, Rutgersson *et al.* 2001). In Guo Larsén *et al.* (2004) the non-dimensional wind gradient

$$\phi_m = \frac{\partial U}{\partial z} \times \frac{\kappa z}{u_*} \, ,$$

is modified for following swell. z is height and $\kappa = 0.4$ is von Karman's constant (Högström 1996).

In this study, new empirical parameterisations are developed for the drag coefficient, taking into account the state of the waves. The data are from a measurement site in the Baltic Sea. A filter-

ing method is developed to reduce the scatter in measured data seemingly connected to irregular low frequency variations. The parameterisations are then implemented and tested in the process-oriented ocean model PROBE-Baltic in a sensitivity study. Since there is no wave information in the model some assumptions are made and we restrict ourselves to compare two runs with different sea states: one run where the expression for growing sea is used, and the other where following swell is assumed for low wind speed. The effect of breaking waves is also implemented in the ocean model for a more reliable description of the ocean surface layer turbulence and surface currents.

Theory

By the MOST the wind speed profile is related to the friction velocity according to:

$$U = \frac{u_*}{\kappa}\left[\ln\frac{z}{z_0} - \psi_m\right] \qquad (3)$$

where ψ_m is the integrated non-dimensional wind gradient (Paulson 1970). The non-dimensional wind gradient ϕ_m is an empirical function of the stability parameter ζ:

$$\zeta = \frac{z}{L} = -\frac{zg\kappa\overline{w'\theta'_v}}{u_*^3 T_0}$$

where L is the Obukhov length and $\overline{w'\theta'_v}$ the buoyancy flux (kinematic flux of virtual temperature) and T_0 is the mean temperature in the surface layer.

Guo Larsén *et al.* (2004) found that ϕ_m is a function of the wave state of the waves. For growing sea ($c_p/U_{10} < 0.8$) and unstable conditions:

$$\phi_m = (1 - 19\zeta)^{-1/4} \qquad (4)$$

which agrees with the recommended expression by Högström (1996) over land. For following swell ($c_p/U_{10} < 1.2$):

$$\phi_m = 1 - (-3\zeta)^{-1/2} \quad -1 < \zeta < 0 \qquad (5)$$
$$\phi_m = -0.73 \quad \zeta < -1$$

In the interval $0.8 < c_p/U_{10} < 1.2$ we usually have a mixture of wave conditions. There are not yet any conclusive results for the ϕ_m in this wave regime and we here use the ϕ_m valid for growing sea.

Using Eqs. 2 and 3 we can express the roughness length as:

$$z_0 = 10\exp\left(-\frac{\kappa}{\sqrt{C_D}} - \psi_m\right) \qquad (6)$$

which can be used to calculate the neutral drag coefficient:

$$C_{DN} = \left(\frac{\kappa}{\ln\dfrac{10}{z_0}}\right)^2 \qquad (7)$$

The drag coefficient C_D is calculated from Eqs. 6 and 7 with:

$$C_{DN} = \left(\frac{\kappa}{\dfrac{\kappa}{\sqrt{C_{DN}}} - \psi_m}\right)^2$$

Measurements

Site and instrumentation

The measurements used in this investigation were taken from the field station at the island of Östergarnsholm. Östergarnsholm is situated about 4 km east of Gotland in the Baltic Sea (at A in Fig. 1). The island has very few trees and is very flat. On the southernmost tip a 30-m tower is erected at about 1 m above the mean sea level. For the wind directions 80–220° the data have been shown to represent open ocean conditions. In a previous analysis of the disturbance in the wave field in combination with a footprint analysis Smedman *et al.* (1999) showed a very small impact of the limited water depth near the shore.

Mean profile data were taken from slow response instruments measuring wind speed and direction and temperature at 5 levels (8, 12.5, 15, 21 and 29 m above mean sea level) and humidity (8 m). Turbulence data were calculated from sonic anemometers Solent 1012R2 at three heights (10, 18 and 26 m) measuring virtual temperature and the three wind components and sampled at 20 Hz. To get 10 m values of wind and temperature the average of the 8 and 12.5 m values were taken.
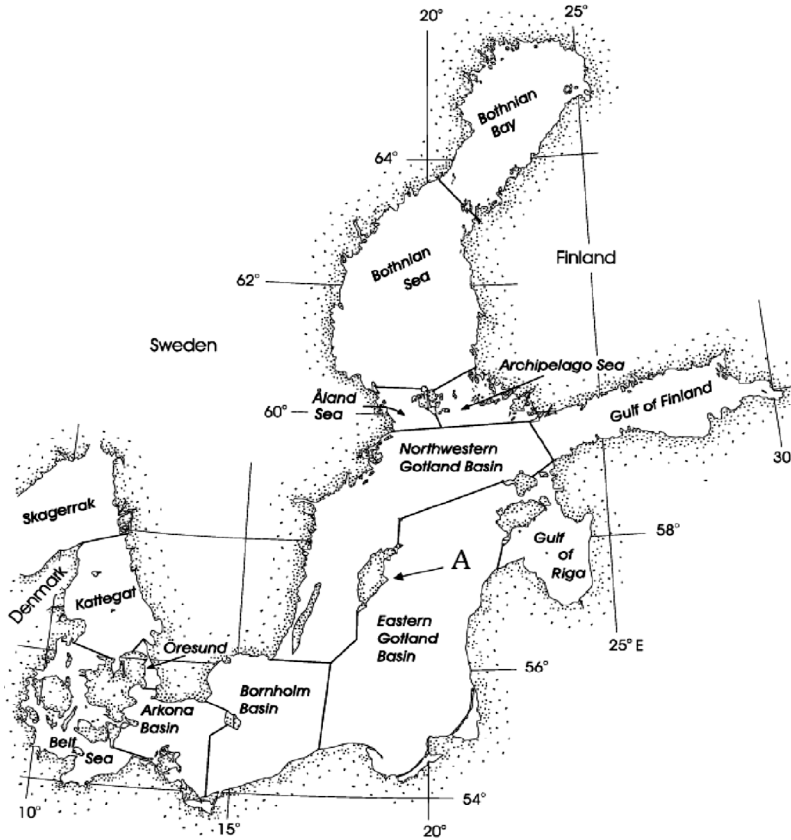
Fig. 1. The Baltic Sea divided into the 13 basins used in the PROBE-Baltic model. The arrow denoted by A shows the position of the Östergarnsholm site.

A wave-rider buoy (run and owned by the Finnish Institute for Marine Research) is moored 3.5 km in the direction of 115° from the tower, giving the wave field and sea surface temperature (SST). For a more detailed description of the site and instrumentation, *see* Smedman *et al.* (1999).

Data were selected using the following criteria: wind from the sector 80–220°, wind speed above 2 m s⁻¹, only upward sensible flux (unstable stratification) and with a dominant wave field from the sector 40–210°. Turbulent fluxes were calculated using the eddy-correlation method and all turbulence statistics were subject to a 10-min running average to remove trends. The data included hourly averages from the period 1995–2004.

Filtering method

The turbulent fluctuations can be illustrated by a spectrum achieved by a Fourier transform on the correlation function. It represents the energy distribution of the components of turbulence in frequency space n. Corresponding fluxes can be described by the cospectrum (real part of the transform). The *uw*-cospectrum C_{uw}, for instance, can be integrated between a selected cut-off frequency n_{lim} and the Nyquist frequency 10 Hz to get the longitudinal part of the kinematic momentum flux.

$$\overline{u'w'} = \int_{n_{lim}}^{10} nC_{uw}d\ln n \qquad (8)$$

The 10-min running average applied to the turbulence data corresponds to a high-pass filter cut-off frequency $n_{lim} \approx 0.0017$ Hz.

The phase shift between the u and w components is described by the phase angle ϕ_{uw} as function of frequency.

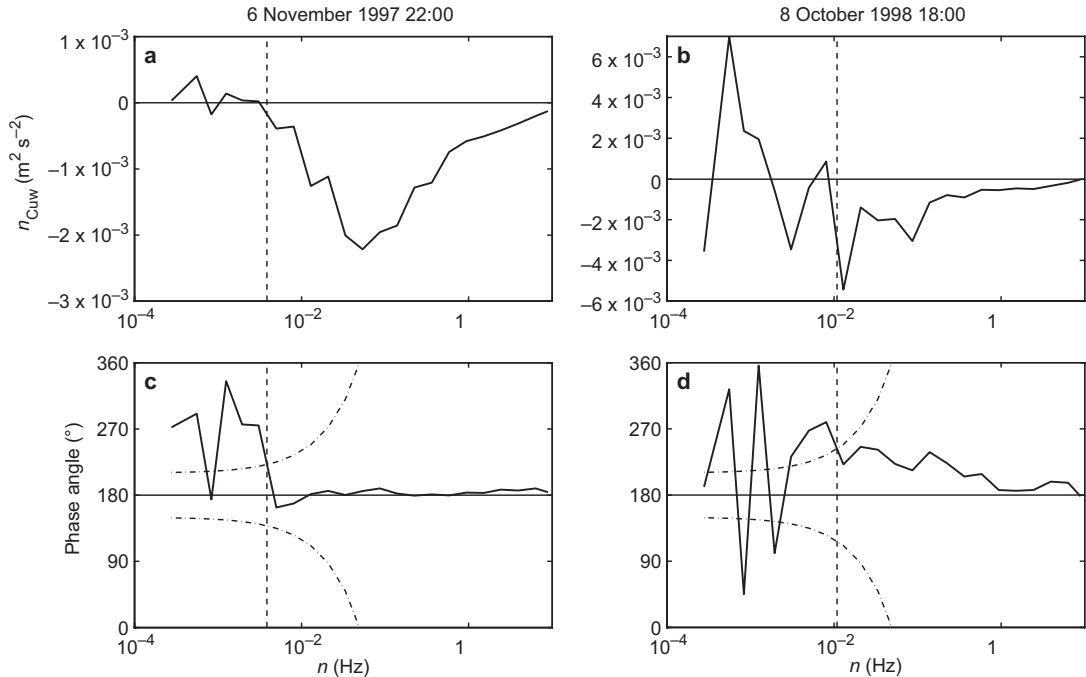$$\phi_{uw}(n) = \tan^{-1}\frac{Q_{uw}(n)}{C_{uw}(n)}$$

Fig. 2. — **a** and **b**: 60-min spectra of the momentum flux $\overline{u'w'}$. — **c** and **d**: The corresponding phase angle for two cases of wind speed between 3 and 4 m s⁻¹. The left-hand side shows a typical growing sea case and the right-hand side a strong swell case. The vertical dashed lines show the used cut-off frequencies in determining the momentum flux (0.004 Hz in left hand side figures and 0.010 Hz in the right hand side figures). The limiting phase angle is shown by the dashed-dotted curves.

Q_{uw} is the quadrature spectrum, i.e. the imaginary part of the Fourier transform (*see* Lumley and Panofsky 1964). For 0° the components are in phase and 180° there is an anti-phase. As the momentum flux is negative, i.e. downwards, we should find the phase angle to be close to 180°. Over land and for growing sea the momentum flux this is generally the case.

One example of a spectrum from 6 Nov. 1997 (Fig. 2a) is shown. The momentum flux was constituted of turbulent fluctuations roughly in the range 0.005 Hz to 10 Hz. The corresponding phase angle between the *u* and *w* components was also near 180° in this range (Fig. 2c). For lower frequencies the spectrum values were close to zero. The small fluctuations at the low frequencies are irregular fluctuations and should not be included when analysing the turbulence. At the transition frequency the phase angle was also seen to change (Fig. 2c). In this case it is rather clear that the cut-off frequency $n_{lim} \approx 0.005$ Hz gives a good estimate of the momentum flux.

However, 0.0017 Hz (10 min) will work as well as the contribution is small between 0.0017 and 0.005 Hz.

When u_* is small, which is the case at low wind speed and during swell, irregular low frequency variations become prominent and influence the cospectra at higher frequencies than 0.0017 Hz (Fig. 2b shows a typical example). These fluctuations do not contribute to the turbulent flux and should not be included when analysing turbulence. These patterns contribute to the large scatter that often is seen in the drag coefficient estimated from measurements during swell. Further, a systematic increase of phase angle with decreasing frequency is seen for higher frequencies (Fig 2d). This type of behaviour is present in many swell cospectra and was identified in Smedman *et al.* (1999) in their analysed period with swell present. This is possibly connected to an indirect swell contribution on the atmospheric turbulence in a broad spectrum band below the frequency of the swell itself.
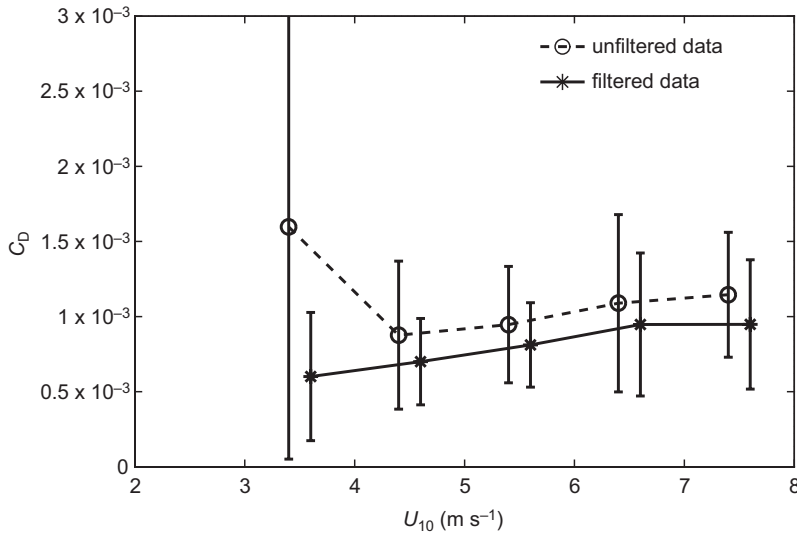
Fig. 3. Calculated drag coefficient C_D during swell. Error bars are standard deviations.

Drennan *et al*. (1999b) also found a swell effect on momentum spectra for frequencies lower than that of the dominant swell waves.

Since we wanted the total surface stress during swell we needed to differentiate between the irregular low frequency variations and the turbulence fluctuations generating stress during swell conditions. This can be done using an Ogive-curve method, by integrating the cospectrum from high to low frequencies (e.g. Guo Larsén *et al*. 2003). In the method presented here the phase angle acted as a steering separator instead.

New cut-off frequencies (replacing the 10-min cut-off) were used if: The phase angle ϕ_{uw} (for each frequency in the range $0.0017 < n < 0.05$ Hz) differed more from 180° than the limiting phase angle ($\phi_{lim} = 30 + 3000n$, dashed-dotted curves in Fig. 2c and d). We chose ϕ_{lim} to be rather large for $n > 0.01$ Hz since this gives the possibility to include the wave effects corresponding to the systematic deviation of the phase angle, mentioned above. The irregular low frequency motions can be filtered out at lower frequencies as ϕ_{lim} is smaller in that region. The cut-off frequency n_{lim} (dashed lines in Fig. 2) was found where $|\phi_{uw} - 180°|$ exceeded ϕ_{lim}, going from higher n. The same procedure was used for C_{vw} using the frequency limits determined for C_{uw}.

The method was applied to all swell data (222 hours). Outliers were removed for non-stationary conditions and if there where single spikes for the

phase angle or in spectra, or if the momentum flux was upward (only one hour). Upward momentum flux is an indication of swell, but present theory cannot include positive momentum flux as u_* then becomes imaginary. Further, only data with angle $\beta < 90°$ between the dominant wave and wind direction were considered, due to limited amount of data with larger angles. The resulting data with swell were 183 hours. The scatter of the drag coefficient C_D (not reduced to neutral) decreased significantly using the filtering method, in particular for $U_{10} < 4$ m s^{-1} (Fig. 3). The mean value of C_D was reduced as well, most significantly for the lower wind speeds.

This method to reduce the irregular low frequency variations gives a similar result to using the Ogive curve, with the advantage that relatively low frequencies affected by the swell can be included. Applying the method for data during growing/mixed sea gave no difference since the irregular variations do not dominate in the same way during these situations (e.g. Fig. 2a and c).

Model

PROBE-Baltic is a process oriented ocean model developed for the Baltic Sea. It is described in detail in Omstedt and Nyberg (1996) and Omstedt and Axell (2003). In the model the Baltic Sea is divided into 13 sub-basins (Fig. 1). Each sub-basin is coupled with surrounding sub-basins
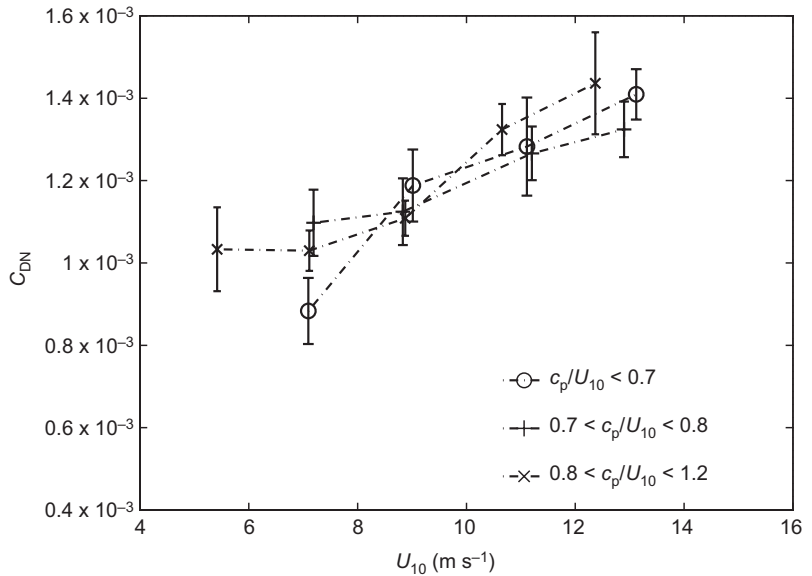
Fig. 4. Neutral drag coefficient C_{DN} for growing/mixed sea conditions calculated from measurements. Data are bin averaged and divided into different wave ages (*see* legend) and the error bars display 95% confidence interval of the mean values.

through in- and outflows. The calculated properties, temperature, salinity and current velocity, are horizontally averaged over each basin. The basins are resolved in the vertical by an expanding grid ranging from 1 m at the boundaries up to 2–10 m, depending on the depth of the basin. Description of the turbulence and the implementation of a wave breaking effect are described in the Appendix. This implementation had a significant impact on both surface currents and the temperature profile.

Input to the model is meteorological data and river runoff together with water-levels in the North Sea. The meteorological forcing, including temperature, geostrophic wind, cloud cover and relative humidity, is from ERA40 data (1958–2001) and the SMHI $(1 \times 1)°$ gridded data set (2002–2004). *See* Omstedt *et al*. (2005) for an evaluation of the difference between the two data sets. The focus in this study is on the eastern Gotland Basin, but the other basins and the Baltic Sea as whole are expected to follow the same pattern. The model was run for the period November 1958 until December 2004.

Results

Parameterisation of C_{DN}

For the parameterisation of the drag coefficient

we focused on the unstable data since influence of swell is not clear for stable data. According to Rutgersson *et al*. (2001) the stability parameter ζ ceases to be a relevant scaling parameter during swell and no systematic variation of C_D with stability can be seen. For the swell data we limited ζ to be equal to –0.4 even when the measured ζ was smaller than –0.4. The neutral drag coefficient was calculated using Eqs. 2, 6 and 7. Equation 4 was used to calculate ϕ_m for both growing and mixed sea ($c_p/U_{10} < 1.2$) and Eq. 5 was used to calculate ϕ_m for all swell data.

The available number of hours with growing or mixed sea conditions was 535. For the growing sea data at $U_{10} > 8$ m s^{-1} there was an indication of higher C_{DN} for the youngest sea as compared with that for the older growing sea data (Fig. 4). This agreed with Drennan *et al*. (2003) who showed higher values for younger seas. The mixed sea, however, gave even higher C_{DN}. Because of the weak wave age dependence at growing/mixed sea C_{DN} was chosen to be a function only of wind speed (Fig. 5):

$$C_{DN} = \max(1.03, 0.60 + 0.060U_{10}) \times 10^{-3} \ (9)$$

The correlation coefficient r for the parameterisation was 0.96.

The relatively limited wave age dependence of C_{DN} was explained in Smedman *et al*. (2003), where it was shown that C_{DN} is not only governed
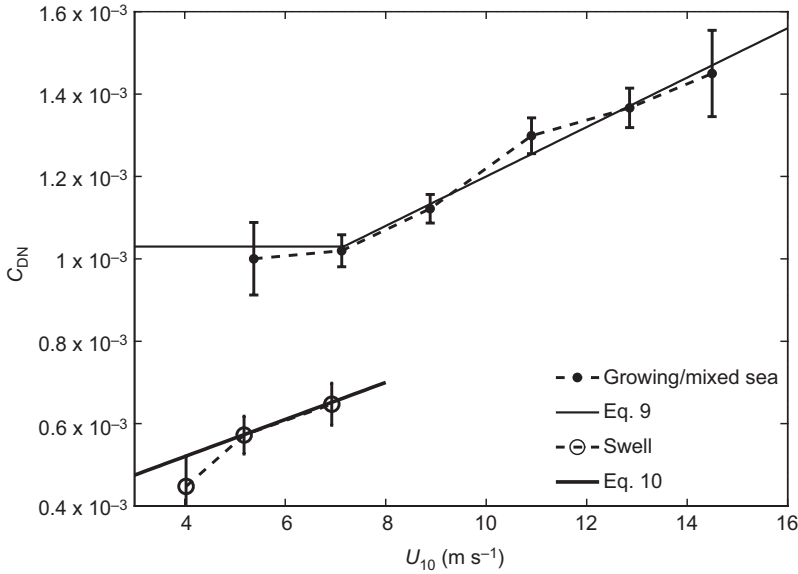
Fig. 5. Neutral drag coefficient C_{DN} for growing/mixed sea and following swell conditions. Data are bin averaged and the error bars display 95% confidence interval of the mean values.

by wave age, but by two parameters representing the wave state, wave age and E_1/E_2. There, E_1 and E_2 were defined as the energy of long waves and short waves, respectively. Thus the relative energy of the long (fast) and short (slow) waves is an important parameter when we want to investigate wave effects in combination with wave age for growing/mixed sea. When lacking information about this parameter we suggest a simple wind speed dependence.

For the swell data with $\beta < 90°$ no variations of C_{DN} with angle could be seen. There is a tendency of higher C_{DN} for $\beta > 90°$, but we have too few data in this regime to draw any further conclusions about the angle dependence of C_{DN}. We thus use the term following swell for $\beta < 90°$ and developed a parameterisation only for that sea state. The neutral drag coefficient during following swell can be described as a function of wind speed only (Fig. 5) according to:

$$C_{DN} = (0.34 + 0.045U_{10}) \times 10^{-3} \qquad (10)$$

The correlation coefficient r for this relation to the data was 0.83. As there were few data for $U_{10} < 4.5$ m s^{-1} it should be remembered that the equation is rather tentative for these conditions. Guo Larsén *et al*. (2003) used partly the same data set (using data from the period 1995–1998) and their result for swell cases is close to our result.

Model results

In the model the equations for the neutral drag coefficient developed from the data in the previous section (Eq. 9 for growing/mixed sea and Eq. 10 for swell) were used together with Eqs. 4 and 5, respectively for the ϕ_m-functions. For all stable conditions Eq. 9 was used. Since no wave information was available in the model we did a sensitivity test of the swell effects. We assumed that swell is present for wind speeds below 8 m s^{-1} and that the wave field was homogeneous in each basin and aligned with the wind. There was no detectable effect in the model of the singularity at 8 m s^{-1}, separating growing/mixed sea from swell. Probably this is more important in a 3-dimensional model than in this in a way 1-dimensional model.

Two runs were simulated and denoted as:

CD$_u$ (reference): .No swell effect included, using Eq. 9 for all wind speeds.

CD$_{w0}$: Following swell ($\beta = 0°$), using Eq. 10 for $U_{10} \leq 8$ m s^{-1} and Eq. 9 for $U_{10} > 8$ m s^{-1}.

When analysing the effect of the new parameterisation in the model only ice-free conditions were used. The 45-year period was used to investigate the long-term impact in the ocean model.

The mean surface stress τ for the eastern Gotland basin was 0.1 N m^{-2} (run CD$_u$). If assum-
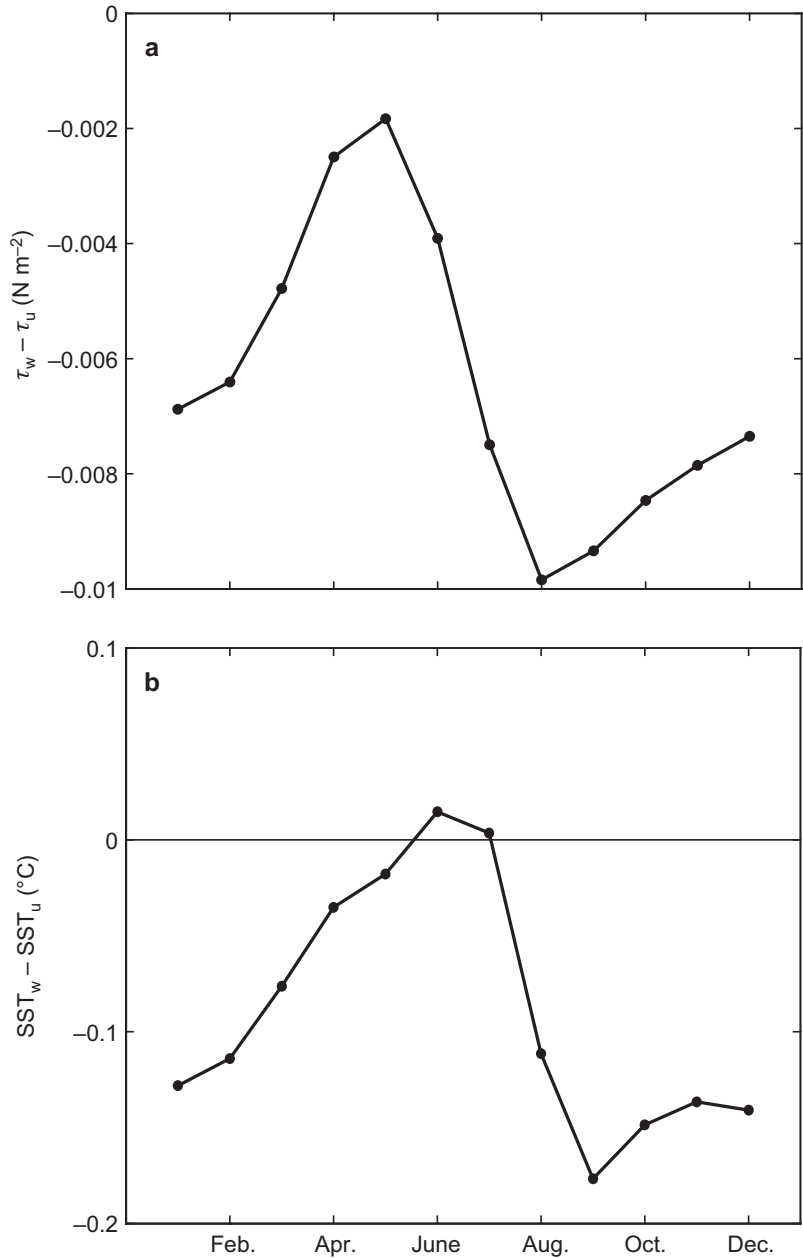
Fig. 6. 45-year mean values for each month of (**a**) the surface stress difference and (**b**) the sea surface temperature differences to the reference run.

ing following swell (run CD_{w0}) the total stress at the surface was reduced by 6%. For situations with winds below 8 m s^{-1} the stress was reduced by 20%. In some situations the assumption of following swell led to a reduction of the stress by more than 50%. Absolute maximum differences to the reference run were about 0.03 N m^{-2}.

The sea surface temperature (SST) was somewhat changed due to a changed mixing of the ocean surface layer. The overall mean SST was,

however, not significantly altered, an average decrease of 0.08 °C for following swell as compared with the reference run. For some periods, though, the difference could be large, exceeding 1 °C, both in terms of cooler and warmer.

For both τ and SST there was a seasonal change in the differences between the following swell and the reference runs. The monthly averaged difference in surface stress was smallest in May (Fig. 6a). At this time the MABL is mostly
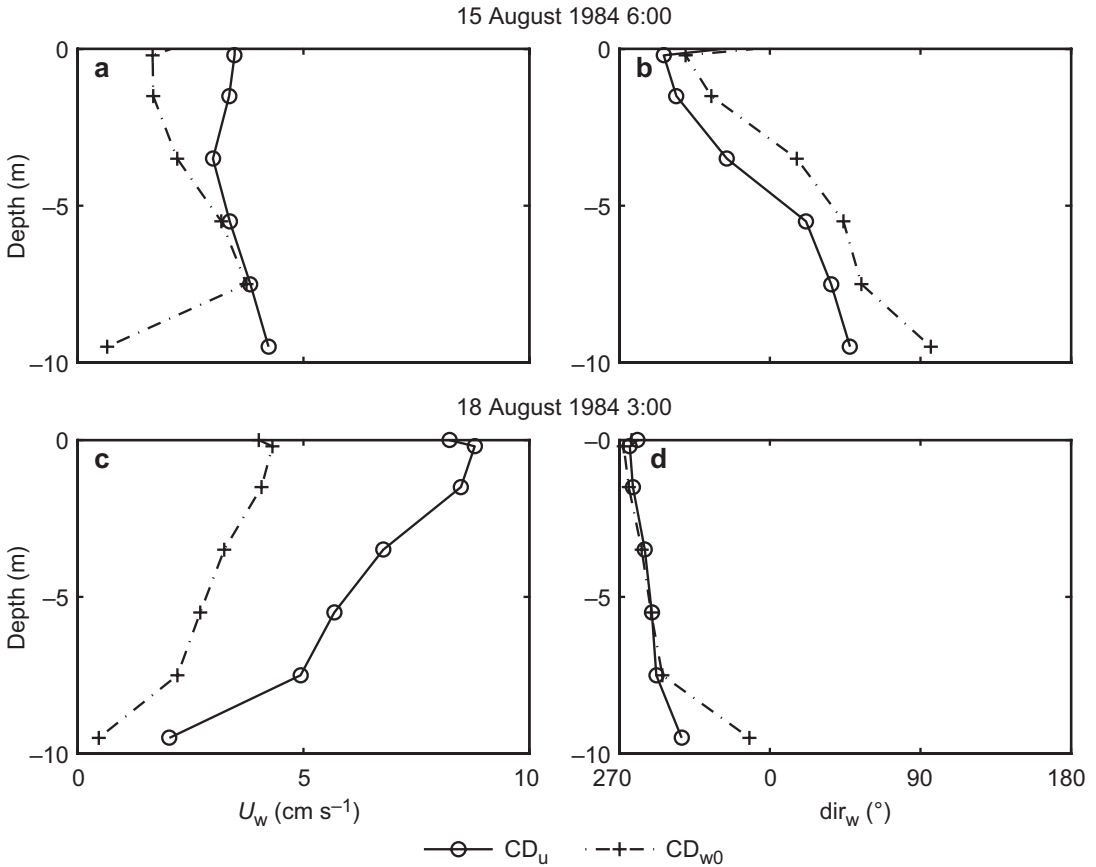
15 August 1984 6:00

18 August 1984 3:00

Fig. 7. Current profiles of speed (left) and direction (right) at two occasions.

stably stratified. The largest difference (on average 0.01 N m^{-2}) was seen in early autumn when it is still relatively weak winds and a starting of longer periods with unstable atmospheric stratification.

The seasonal pattern in SST difference to the reference run was smaller than 0.2 °C (Fig. 6b). There was a small increase in temperature during June–July and a decrease in early autumn. The reason behind the seasonal change in SST difference was the yearly change in the temperature profile in the water. The mean effects on the mixing depth in the sea were limited.

The current velocity was on average only slightly influenced. The surface current speed was in mean reduced by 1% when assuming following swell. For situations with wind speed below 8 m s^{-1} the reduction was 4%. At 5-m depth the reduction was 7% for the same wind speed interval. In absolute values this means

differences measured in mm s^{-1}. However, there were occasions where both speed (Fig. 7a and c) and direction (defined as where the current comes from, Fig. 7b and d) differed considerably. For extreme cases the difference in speed could be of the order dm s^{-1} (not shown).

Discussion

The parameterisation

There have been a number of studies focusing on the air–sea exchange of momentum. Most of them agree on a wind dependence of C_{DN} (Fig. 8). The widely used COARE 3.0 algorithm (Fairall *et al*. 2003) can be considered present state of the art. Large and Pond's (1981) classical curve is constant below 10 m s^{-1} and increases linearly with wind speed above. The neutral drag
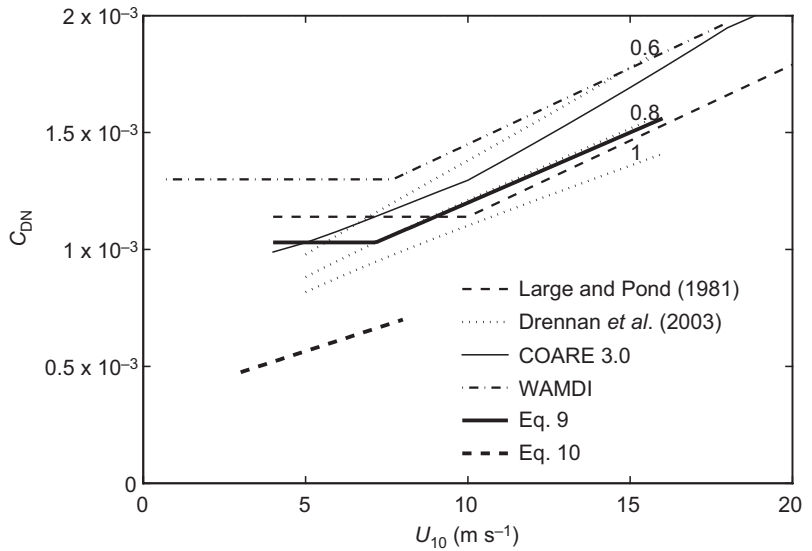
Fig. 8. The neutral drag coefficient from different studies. The numbers next to the lines (Drennan *et al.* 2003) represent wave age.

coefficient by the WAMDI Group (Janssen *et al.* 1987, WAMDI Group 1988) is often used for wave modelling. This expression is used in the original version of PROBE-Baltic. It is higher than the other curves discussed. Drennan *et al.* (2003) presented a wave age dependent neutral drag coefficient.

The result of the present study is also shown in Fig. 8. Our growing/mixed sea parameterisation follows the 0.8-wave age line of Drennan *et al.* (2003) for $U_{10} > 7$ m s^{-1} and near the curve of Large and Pond (1981) for $U_{10} > 8$ m s^{-1}.

Our result on the following swell conditions is close to the result of Drennan *et al.* (1999a) who got $C_{DN} \approx 0.7 \times 10^{-3}$ at $U_{10} \approx 7$ m s^{-1} during a following swell case (not shown). The slightly smaller values in this study can be explained by the use of the ϕ_m-expression valid for swell, which has a significant influence on C_{DN} calculated from measurements.

The model simulations

Including the swell effect on the stress description in the PROBE-Baltic model did not alter the ocean mixed layer depth significantly as a long term average. This depth is mainly governed by the turbulent mixing of the ocean surface layer and the heat fluxes at the surface, together with the halocline (during winter). It is probably

more influenced by high-wind situations than the low-wind situations when swell is present. In addition the turbulence in the ocean is mainly considered to be generated as well as dissipated near the surface.

For ocean current velocity the importance of swell is somewhat larger. In the modelling of dispersion of oil or biomass transport, for instance, it could be crucial to model the currents correctly. One should bear in mind here that this model is not suitable for current modelling as this parameter is unrealistically averaged over whole basins. It is primarily used as a parameter determining the turbulence. To do a realistic quantification of the impact of swell on the current velocity one should instead use a horizontally well-resolved model.

The use of the new expression for growing sea (Eq. 9) gave on average 18% lower stress as compared with that for the original setting in the model with the WAMDI formulation (*see* the previous sub-section). Large seasonal differences in the SST were also seen and the ocean mixing depth was changed due to this. Currents were almost completely different. This shows that the model is not insensitive to a change in the drag coefficient.

We included the wave breaking effect in the PROBE-Baltic model with the presumption that this effect was important to have in the model to be able to do a correct analysis of the impact of

swell. Yet, the wave breaking effect did not significantly change the impact of swell on the SST in the model. The surface currents, however, were very much dependent on a correct turbulence description.

Conclusions

During swell, i.e. when the dominant sea waves travel faster than the wind, the turbulence structure in the atmosphere is changed, as compared with growing sea conditions and over land. Among other processes the wind stress is altered. For wind following swell the stress is lowered and for counter swell the stress is enhanced as compared with those for growing sea conditions. A method to reduce the scatter in swell data of the neutral drag coefficient was developed and filters out irregular low frequency variations. Using the filtered data two new expressions of the drag coefficient were developed discriminating between growing/mixed sea and wind following swell (Eq. 10 for swell). The new expressions were implemented in the process oriented ocean model PROBE-Baltic to investigate the effect of swell on the oceanic surface layer. Since no wave model was included we did a sensitivity test with two runs, one reference with only growing/mixed sea, and one assuming following swell, when the wind speed was lower than 8 m s^{-1}. The model was run for 45 years. The results give a measure of the maximum influence from swell in the Baltic Sea but information about waves is needed to compare the results to observations.

The main results are:

- For the 45-year average the surface stress was reduced by 6% for wind following swell. Below 8 m s^{-1} the stress was reduced by 20%.
- Current velocity was altered during periods with low wind speed, occasionally of the order dm s^{-1}. However, to realistically quantify this impact one needs a horizontally well-resolved ocean model.
- The temperature and the mixing depth in the ocean were not significantly changed.

To conclude, the implementation of the swell effect is of limited importance for a process oriented ocean model. There is an indication that current velocity is the most sensitive parameter. It is likely that the impact of swell is larger in the atmosphere.

References

Axell L.B. & Liungman O. 2001. A one-equation turbulence model for geophysical applications: comparison with data and the *k-ε* model. *Env. Fluid Mech.* 1: 71–06.

Burchard H. 2001. Simulating the wave-enhanced layer under breaking surface waves with two-equation turbulence models. *J. Phys. Oceanogr.* 31: 3133–3145.

Businger J.A., Wyngaard J.C., Izumi Y. & Bradley E.F. 1971. Flux-profile relationships in the atmospheric surface layer. *J. Atm. Sci.* 28: 181–189.

Charnock H. 1955. Wind stress on a water surface. *Q. J. R. Meteorol. Soc.* 81: 639–640.

Craig P.D. & Banner M.L. 1994. Modeling wave-enhanced turbulence in the ocean surface layer. *J. Phys. Oceanogr.* 24: 2546–2559.

Donelan M.A. 1990. Air–sea interaction. In: LeMehaute B. & Hanes D. (eds.), *The sea: ocean engineering science*, vol. 9, John Wiley, New York, pp. 239–292.

Drennan W.M., Graber H.C. & Donelan M.A. 1999a. Evidence for the effects of swell and unsteady winds on marine surface stress. *J. Phys. Oceanogr.* 29: 1853–1864.

Drennan W.M., Kahma K.K. & Donelan M.A. 1999b. On momentum flux and velocity spectra over waves. *Boundary-Layer Meteorol.* 92: 489–515.

Drennan W.M., Graber H.C., Hauser D. & Quentin C. 2003. On the wave age dependence of wind stress over pure wind seas. *J. Geophys. Res.* 108 (C3), doi: 10.1029/2000JC000715.

Fairall C.W., Bradley E.F., Hare J.E., Grachev A.A. & Edson J.B. 2003. Bulk parameterization of air–sea fluxes: updates and verification for the COARE algorithm. *J. Climate.* 16: 571–591.

Grachev A.A. & Fairall C.W. 2001. Upward momentum transfer in the marine boundary layer. *J. Phys. Oceanogr.* 31: 1698–1711.

Guo Larsén X., Makin V.K. & Smedman A.-S. 2003. Impact of waves on sea drag: measurements in the Baltic Sea and a model interpretation. *The Global Atmosphere and*

Ocean System. 9: 97–120.

Guo Larsén X., Smedman A.-S. & Högström U. 2004. Air–sea exchange of sensible heat over the Baltic Sea. *Q. J. R. Meteorol. Soc.* 130: 519–539.

Haugen D.A., Kaimal J.C. & Bradley E.F. 1971. An experimental study of Reynolds stress and heat flux in the atmospheric surface layer. *Q. J. R. Meteorol. Soc.* 97: 168–180.

Högström U. 1990. Analysis of turbulence structure in the surface layer with a modified similarity formulation for near neutral conditions. *J. Atm. Sci.* 47: 1950–1972.

Högström U. 1996. Review of some basic characteristics of the atmospheric surface layer. *Boundary-Layer Meteorol.* 78: 215–246.

Holland J.Z., Chen W., Almazon J.A. & Elder F.C. 1981. Atmospheric boundary layer. In: Aubert E.J. & Richards T.L. (eds.), *IFYGL — The international field year for the Great Lakes*, NOAA, Ann Arbor, Mich., pp. 109–167.

Janssen P.A.E.M., Komen G.J. & de Voogt W.J.P. 1987. Friction velocity scaling in wind wave generation. *Boundary-Layer Meteorol.* 38: 29–35.

Large W.G. & Pond S. 1981. Open ocean momentum flux measurements in moderate to strong winds. *J. Phys. Oceanogr.* 11: 324–336.

Lumley J.L. & Panofsky H.A. 1964. *The structure of atmospheric turbulence*. Wiley-Interscience, New York.

Mellor G. & Blumberg A. 2004. Wave breaking and ocean surface layer thermal response. *J. Phys. Oceanogr.* 34: 693–698.

Omstedt A. & Nyberg L. 1996. Response of Baltic Sea ice to seasonal, interannual forcing and climate change. *Tellus* 48A: 644–662.

Omstedt A. & Axell L.B. 2003. Modeling the variations of salinity and temperature in the large gulfs of the Baltic Sea. *Cont. Shelf Res.* 23: 265–294.

Omstedt A., Chen Y. & Wesslander K. 2005. A comparison between the ERA40 and the SMHI gridded meteorological databases as applied to Baltic Sea modelling. *Nordic Hydrol.* 36: 369–380.

Paulson C.A. 1970. The mathematical representation of wind speed and temperature profiles in the unstable atmospheric surface layer. *J. Appl. Meteorol.* 9: 857–861.

Pierson W.J. 1964. The interpretation of wave spectrums in terms of the wind profile instead of the wind measured at a constant height. *J. Geophys. Res.* 69: 5191–5203.

Pierson W.J. & Moskowitz L. 1964. A proposed spectral form for fully developed seas based on the similarity theory of S.A. Kitaigorodskii. *J. Geophys. Res.* 69: 5158–5190.

Rutgersson A., Smedman A.-S. & Högström U. 2001. Use of conventional stability parameters during swell. *J. Geophys. Res.* 106 (C11): 27117–27134.

Rutgersson A. & Sullivan P.P. 2005. The effect of idealized water waves on the turbulent structure and kinetic energy budgets in the overlying airflow. *Dynamics of Atm. and Oceans.* 38: 147–171.

Smedman A.-S., Tjernström M. & Högström U. 1994. The near-neutral marine atmospheric boundary layer with no surface shearing stress: a case study. *J. Atm. Sci.* 51: 3399–3411.

Smedman A.-S., Högström U., Bergström H., Rutgersson A., Kahma K.K. & Pettersson H. 1999. A case study of air-sea interaction during swell conditions. *J. Geophys. Res.* 104(C11): 25833–25851.

Smedman A.-S., Guo Larsén X., Högström U., Kahma K.K & Pettersson H. 2003. Effect of sea state on the momentum exchange over the sea during neutral conditions. *J. Geophys. Res.* 108 (C11), doi: 10.1029/2002JC001526.

Stacey M.W. 1999. Simulation of the wind-forced near-surface circulation in Knight Inlet: a parameterization of the roughness length. *J. Phys. Oceanogr.* 29, Notes and Correspondence: 1363–1367.

Sullivan P.P., McWilliams J.C. & Moeng C.-H. 2000. Simulation of turbulent flow over idealized water waves. *J. Fluid Mech.* 404: 47–85.

Sullivan P.P., Edson J.B., Hristov T. & McWilliams J.C. 2008. Large-eddy simulations and observations of atmospheric marine boundary layers above nonequilibrium surface Waves. *J. Atm. Sci.* 65: 1225–1245.

Terray E.A., Drennan W.M. & Donelan M.A. 1999. The vertical structure of shear and dissipation in the ocean surface layer. In: Banner M.L. (ed.), *The wind-driven air–sea interface*, School of Mathematics, University of New South Wales, Sydney, Australia, pp. 239–245.

Umlauf L., Burchard H. & Hutter K. 2003. Extending the k-ε turbulence model towards oceanic applications. *Ocean modelling* 5: 195–218.

WAMDI Group [Hasselmann S., Hasselmann K., Bauer E., Janssen P.A.E.M., Komen G., Bertotti L., Lionello P., Guillaume A., Cardone V.C., Greenwood J.A., Reistad M., Zambresky L. & Ewing J.A.] 1988. The WAM model — a third generation ocean wave prediction model. *J. Phys. Oceanogr.* 18: 1775–1810.

Appendix

The turbulence in the PROBE-Baltic model is described by a k-ε model. The transport equations for the turbulent kinetic energy (TKE) $k = \sum_{i=1}^{3} 0.5u_i^2$, where u_i are the velocity components, and dissipation rate ε are explicitly solved (Axell and Liungman 2001).

The upper boundary conditions for the TKE and dissipation are

$$k = \left[(1+c_{\mathrm{w}}) \frac{u_\tau^3}{\left(c_\mu^0\right)^3} + \frac{\max\left(B,0\right)l}{\left(c_\mu^0\right)^3} \right]^{\frac{2}{3}} \tag{A1}$$

$$\varepsilon = \left(c_\mu^0\right)^3 \frac{\kappa^{\frac{3}{2}}}{l} \tag{A2}$$

Here

$$u_\tau = \sqrt{\frac{\tau}{\rho_0}}$$

is the ocean friction velocity, where $\rho_0 = 1000$ kg m^{-3} is the water density. B is the buoyancy flux at the boundary and $l = -\kappa z$ is the turbulent macro scale. $c_\mu^0 \approx 0.55$ is a constant and in the original version of the model the wave breaking parameter $c_{\mathrm{w}} = 0$.

The boundary conditions for the current speed are:

$$v_{\mathrm{T}} \frac{\partial u}{\partial z} = u_\tau^2 \tag{A3}$$

$$v_{\mathrm{T}} \frac{\partial v}{\partial z} = 0 \tag{A4}$$

where u and v are the current velocity components in the mean wind direction and lateral direction, respectively, and v_{t} is the eddy diffusivity, depending on k, l and stability in the water. The surface stress t is determined from the bulk relation in Eq. 2.

If including wave breaking one introduces a surface roughness length z_{w} for the water side in $l = \kappa(-z + z_{\mathrm{w}})$ (Craig and Banner, 1994). It is parameterised in the model as $z_{\mathrm{w}} = H_{\mathrm{s}} = 114\,u_{\mathrm{t}}$ (Stacey 1999 and L. B. Axell pers. comm.) where H_{s} is the significant wave height. The parameter z_{w} should not be seen as a physical roughness length but rather as a length scale of the injected turbulence by the breaking waves (Umlauf *et al.* 2003).

One further assumes a balance between dissipation and diffusion (flux of TKE from the surface). For the turbulence input by the wave breaking we then have

$$\frac{v_{\mathrm{T}}}{\sigma_{\mathrm{k}}} \frac{\partial \kappa}{\partial z} = m u_\tau^3 \tag{A5}$$

The constant $m = 100$ is called the "wave energy factor" (Craig and Banner 1994). We can then determine c_{w} in Eq. A1 ($\sigma_{\mathrm{k}} = 1$):

$$c_{\mathrm{w}} = \sqrt{\frac{3\sigma_{\mathrm{k}}}{2}} c_\mu^0 m = 67 \tag{A6}$$

according to Burchard (2001) where our c_{w} refers to the whole second term inside the bracket at $z = 0$ in his eq. 12 and that his c_μ^0 is defined as our $(c_\mu^0)^4$.

There are some uncertainties in this approach. The parameterisation for z_{w} according to significant wave height, for instance, ranges from at least $0.5H_{\mathrm{s}}$ to $1.6H_{\mathrm{s}}$ (Terray *et al.* 1999, Burchard 2001). As the model does not include a wave model the uncertainty increases as H_{s} itself must be parameterised. Further, z_{w} can also be described by the Charnock relation with a much larger Charnock parameter

α than used for the atmosphere. This α varies as well between different studies (e.g. Stacey 1999, Mellor and Blumberg 2004).

The model was run both excluding and including the wave breaking effect. The surface values and the gradient of the current speed close to the surface decreased due to the enhanced mixing from the injected turbulence by the breaking waves. A near logarithmic profile was achieved when no wave breaking was implemented. There was a change from the surface to the bottom giving larger temperature differences between bottom water and surface water when wave breaking was included and in addition a shallower ocean mixed layer was seen. This means that the turbulence intensity decreases rapidly near the surface. One of the sources of turbulence vanishes as the gradient decreases. Bothnian Bay showed an even more distinct change of profile and mixed layer depth. On a 45-year basis there was a mean increase of SST by nearly 0.1° and damped extreme temperatures in the summer (0.5 °C) in the eastern Gotland basin.